Thermal Profiling Using Infrared Thermography in Friction Surfacing

H. KHALID RAFI, KRISHNAN BALASUBRAMANIAM, G. PHANIKUMAR, and K. PRASAD RAO

Infrared (IR) thermography was used to measure thermal profiles in the coating, consumable rod, and substrate during friction surfacing. A sudden raise followed by a steady state in thermal profile was observed and attributed to viscous heat dissipation during plastic deformation. The retreating side of the coating experienced higher temperature compared to the advancing side, indicating that the hot plasticized metal is carried from the advancing side to the retreating side.

DOI: 10.1007/s11661-011-0750-8

I. INTRODUCTION

FRICTION surfacing is a solid-state technique to produce relatively thick coatings for wear and corrosion applications. The process does not involve melting and many of the limitations associated with a fusion-based technique can be overcome.

A schematic of the friction surfacing process and a typical friction surfaced stainless steel coating on steel substrate are shown in Figure 1. A rotating consumable rod was fed against a substrate with simultaneous axial force acting on the rod. Once the rubbing end of the consumable rod was sufficiently plasticized, the substrate was traversed horizontally with respect to the vertical consumable rod. Consequently, the plasticized material gets coated over the substrate by a combined effect of axial load and substrate traverse.[1] The capability to coat a variety of materials on different substrates makes this process attractive.[2]

Peak temperature at the interface and the thermal profiles in the region near the interface can significantly affect coating formation, heat-affected zone microstructure, and interfacial bond strength. In order to develop friction surfacing as an acceptable coating process, it is necessary to understand the thermal phenomena that take place during the entire process of coating formation. The main aim of this work is to determine the temperature distributions in the coating, the consumable rod, and the substrate using infrared (IR) thermography.

IR thermography is a convenient, noncontact method for measurement of temperature fields. An IR camera was used for temperature measurement in the past for heat-transfer studies.[3] Availability of highly sensitive photon detectors and related electronics in recent years made the IR camera measurements more accurate and precise. In the last decade, this technique was used for different applications such as welding, fracture studies, plastic deformation studies, nondestructive flaw testing, fluid dynamic studies, and medical related studies.[4] In welding, the measured temperature data were used to calibrate the simulation results and to compare different metal joining processes such as laser welding, laser brazing, and laser-MIG hybrid welding.[5–8] IR thermography was widely used for characterizing fatigue behavior of steels and to measure the temperature rise on aluminum alloys caused by high stress levels during the low-cycle fatigue tests.[9] Paoloni *et al.* used IR thermography for the characterization of residual stress in plastically deformed metallic components. The method is based on the evaluation of thermal diffusivity, which is dependent on the local dislocation density in the material lattice induced by plastic deformation.[10] Another area in which IR camera measurements were frequently used was for nondestructive flaw detection. Here, the heat flux delivered onto a sample surface by an external source propagates in-depth and experiences specific disturbances on the defect regions.[11] The recent developments in IR camera measurements show its potential to consider it as a reliable technology for temperature measurements.

In friction surfacing, it is important to know the temperature developed at different stages to get a basic understanding about the process. Reported studies in the open literature on thermal profiles during friction surfacing processes are limited. Bedford *et al.*[12] showed that the temperature reached at the consumable rod/substrate interface was about 1273 K (1000 °C) for high speed steel consumable rod, whereas Liu *et al.*[13] estimated temperatures close to 1623 K (1350 °C) for stainless steel (AISI 321) consumable rod by mathematical modeling. In this work, an approach based on IR measurement was used to generate thermal profiles during the friction surfacing process.

H. KHALID RAFI, PhD Scholar, G. PHANIKUMAR, Associate Professor, and K. PRASAD RAO, Professor, are with the Materials Joining Laboratory, Department of Metallurgical and Materials Engineering, Indian Institute of Technology Madras, Chennai 600 036, India. Contact e-mail: khalidrafi@gmail.com KRISHNAN BALASUBRAMANIAM, Professor, is with the Machine Design Section, Department of Mechanical Engineering, Indian Institute of Technology Madras.

Manuscript submitted January 29, 2011.
Article published online June 9, 2011

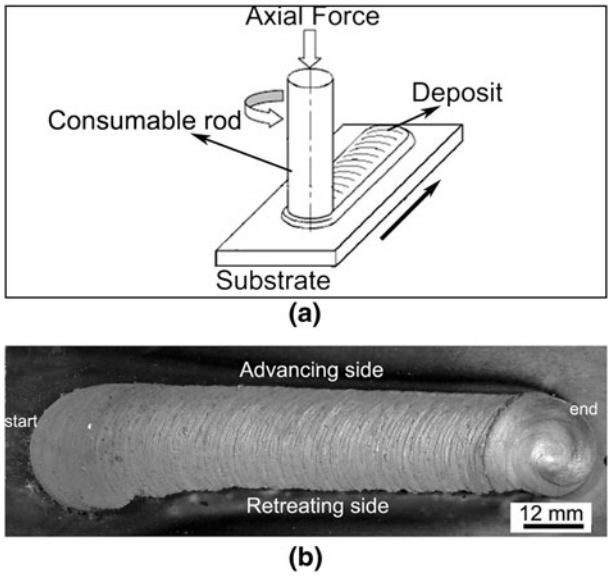

Fig. 1—(*a*) Schematic of the friction surfacing process. The left end of the schematic is termed the "advancing side," and the right end is termed the "retreating side." (*b*) Typical AISI 304 friction surface coating on the steel substrate.

II. EXPERIMENTAL PROCEDURE

Friction surfacing experiments were carried out in a custom designed friction surfacing machine capable of delivering 10 kN axial load and spindle rotation speed of 3000 rpm. AISI 304 (18-mm diameter and 100-mm length) with chemical composition (wt pct) C0.081, Cr17.75, Ni7.70, Mn1.17, Si0.77, and balance Fe was used as consumable rod. Low carbon steel (AISI 1012) (200 mm × 150 mm × 10 mm) was used as a substrate material. The following friction surfacing parameters were used: axial load = 10 kN, substrate traverse speed = 4 mm/s, and consumable rod rotation speed = 800 rpm. Coating of 80-mm length was produced and temperature measurements were carried out during the entire process.

The high speed rotation of the consumable rod precludes the measurement of temperature using the conventional thermocouple method. Though wireless thermocouples could be used, locating the thermocouples near the rubbing interface is not practicable as the consumable rod progressively gets consumed. In this study, a more efficient experimental method, IR thermography, was used to generate the thermal profiles during friction surfacing. An IR camera with a mean noise equivalent temperature difference of 20 mK was used to measure the surface temperature for all the welding experiments. The CEDIP JADE mercury cadmium telluride camera (M\S. Flir System, Croissy-Beaubourg, France) is operated in the long wave infrared band (7.9 to 9.7 μm) with a focal plane array of 320 × 240 detectors (each detector is a pixel of size is 25 μm) and a pixel pitch of 30 μm. The IR camera measures temperature variations based on irradiance of an object surface. The image data can be calibrated and expressed as location-dependent temperature.

III. THERMAL CALIBRATION OF IR CAMERA

The detected photons from the object have to be assigned to a corresponding temperature to measure the absolute observing surface temperature correctly. The thermographic calibration of an IR system is carried out by measurements based on effective blackbody radiance and temperature. The relation between the temperature of an object and the radiation focused on the detector depends on the emissivity of the surface of the object. Every IR camera designed for absolute temperature measurements is calibrated by taking a number of blackbody measurements at known temperatures, radiance levels, emissivities, and distances. The IR camera is calibrated with the following steps.

(1) The blackbody device is heated to different known temperature levels, and the corresponding blackbody radiation is captured by the IR camera through its lens. (The emissivity of the blackbody used lies between 0.96 and 0.98.)
(2) The photon detector collects these photons and produces signal voltage (using an A/D converter) that results in a digital count.
(3) The digital counts obtained from multiple readings are fed into calibration software (CEDIP JADE Camera is equipped with "Altair" Calibration software). Based on the digital counts and the known temperatures taken at different instances, the software creates a series of calibration curves that are stored in the camera system's memory as a series of numeric curve-fit tables that relate radiance values to blackbody temperatures.
(4) When the system makes a measurement, it takes the digital value of the signal at a given moment, uses an appropriate calibration table, and calculates absolute surface temperature.

The IR camera used in this study was calibrated to measure the temperature up to 1773 K (1500 °C).

IV. METHOD OF TEMPERATURE MEASUREMENT

The calibrated IR camera is placed at an appropriate distance (0.5 m) from the surfacing zone and focused to the surfacing region. The IR camera used for the study and the locations where the camera was placed are shown in Figure 2. The number of detectors exposed to the radiation of the observed IR scene depends on the size of the field of view selected. All the detectors (320 × 240) will be exposed at the same time if full window is selected. For the current study, quarter windows as well as customized windows were selected as the field of view. The two-dimensional size of the total field of view (TFOV) is given by the following relationship:

$$\mathrm{TFOV(hor)} = \frac{N_{(\mathrm{hor})} \cdot d_{(\mathrm{obj})} \cdot P \cdot 10^{-6}}{d_{(\mathrm{foc})}}$$

$$\mathrm{TFOV(ver)} = \frac{N_{(\mathrm{ver})} \cdot d_{(\mathrm{obj})} \cdot P \cdot 10^{-6}}{d_{(\mathrm{foc})}}$$

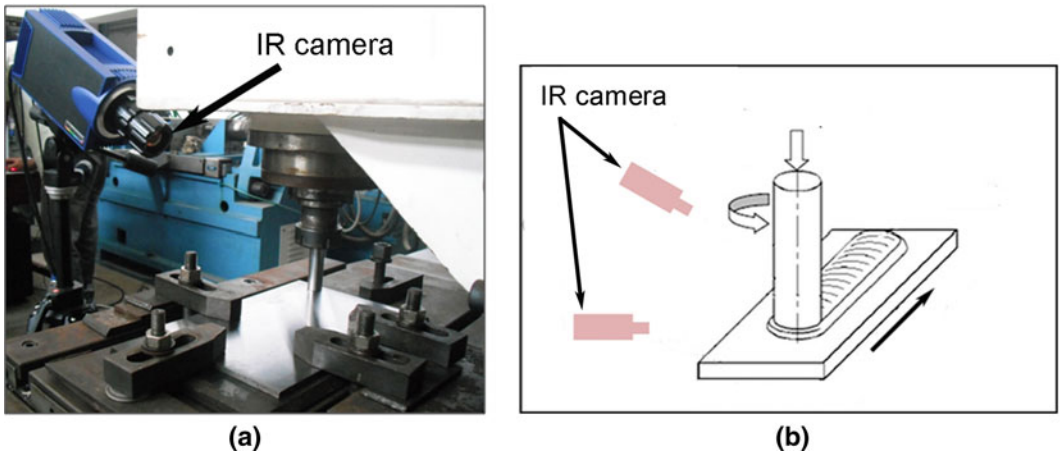

Fig. 2—(*a*) IR camera used for the study (shown by arrow). (*b*) IR camera positions.

where TFOV (hor) and TFOV (ver) are the total field of view in the horizontal and vertical (m) directions, respectively; N_{hor} and N_{ver} are the horizontal and vertical pixel numbers; d_{obj} is the working distance between the lens and the object (m); P is the pitch (μm); and d_{foc} is the focal distance (m).

Once the field of view was set, the IR camera was subjected to nonuniformity correction (NUC). This was done by exposing the detectors first to a blackbody at room temperature and then to a uniformly heated plate. This procedure ensures the same energy levels for all the detectors before the start of the experiment.

The thermal images were captured as continuous frames. Thermal images can be acquired rapidly, and a rate of 200 frames per second was used to ensure sufficient sampling of the temperature values. The higher frame rate effectively nullifies the diffusivity effects at higher operating temperatures. An integration time (the time required for processing individual frames) of 30 μs was set, and the lens of focal length 25 mm was used to capture the thermal images.

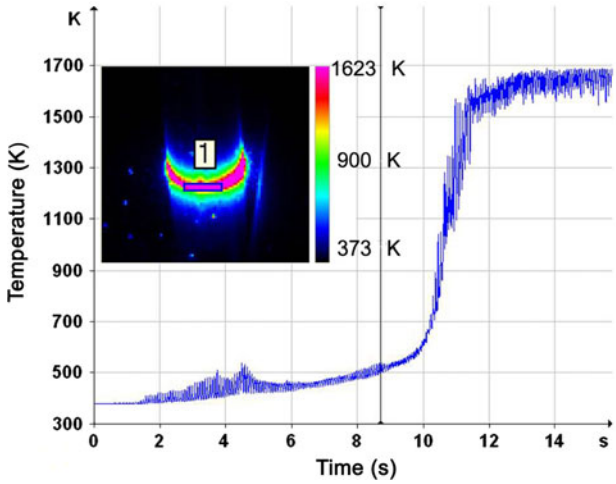

Fig. 3—Thermal profile (the average temperature in the boxed region) as a function of time during the heating stage. (The corresponding thermogram at a time-step is also shown in the insert image.)

V. RESULTS AND DISCUSSION

Figure 3 shows the time-temperature plot at the consumable rod/substrate interface during the heating phase. A gradual increase in temperature was observed for a certain period of time (up to 10 seconds) followed by a transient phase, during which the temperature increased rapidly to higher levels. Once the peak temperature [1573 K (1300 °C)] was attained, the process reached a steady state. The gradual increase in temperature was due to the frictional heating. The mechanism of temperature rise during the transient phase can be attributed to viscous dissipation during plastic deformation preceded by adhesion due to direct metal to metal contact between the two nascent surfaces.

The local interfacial heat generation due to friction depends on the frictional force and the sliding velocity. The interfacial heat generation due to deformation can be modeled as a product of shear stress and velocity of the plasticized consumable rod material, which rotates along with the consumable rod. The rate of localized heat generation (de) can thus be approximated as follows:[14]

$$de = \delta(\omega r - U\sin\theta)\mu_f p dA + (1-\delta)(\omega r - U\sin\theta)\tau_Y dA$$

Here, δ is the extent of slip; ω is the angular velocity at which the consumable rod rotates; r is the radial distance from the tool axis; U is the substrate traverse speed; θ is the angle between the radial vector, r, and the coating direction; μ_f is the friction coefficient; p is the local pressure applied by the consumable rod on the elemental area dA; and τ_Y is the shear yield stress related to that in tension (σ_Y) by the von Mises criterion $\tau_Y = \sigma_Y/\sqrt{3}$.[14]

When δ is 1, no material sticks to the tool and all the heat is generated by friction due to sliding. In contrast, when $\delta = 0$, all the heat is generated by plastic deformation. The steep temperature gradient observed in Figure 3 suggests a transition of sliding to sticking after about 10 seconds, which means that the extent of

slip, δ, tends to zero after 10 seconds and the heat generation thereafter is not due to friction. Once sticking occurs, heat is generated at the consumable rod–substrate interface by plastic deformation. During sticking, the metal to metal contact leads to development of a peak torque resistance, which resulted in a surge in temperature at the localized region. Hence, the flow stress of the material close to the contact region comes down and, consequently, the material becomes softened. It should be noted that the heat localization was greater toward the consumable rod than the substrate owing to the large difference in their size. Due to the continuous action of the axial force, the softened metal undergoes severe plastic deformation. The peak temperature attained during the transient phase sustains until the end of the process because of plastic deformation and viscous heat dissipation.[15] This study suggests that the value for δ in a numerical simulation cannot be chosen arbitrarily at a constant value but is actually a function of time during the dwell period and is likely to be zero later.

Figure 4 shows the temperature distribution along the rotating consumable rod from the contact surface toward the clamping region. The rate of heating is faster at regions closer to the interface. A higher thermal gradient between the plasticized region close to the interface and the rest of the consumable rod will ensure a steady-state thermal profile and a stable coating process. For the material used in this study (AISI 304), the thermal conductivity is suitably high for the required friction surfacing conditions. Earlier attempts with copper and aluminum as coating consumables were not readily successful, which could be attributed to high thermal conductivity of the consumable rod material and the consequent instability of flow at the rod-substrate interface.

To obtain the thermal profile from the top surface to the bottom of the substrate, coating was made along one of the extreme edges of the substrate. The IR camera was placed in such a way that the focus can be made on the transverse surface of the substrate. Figure 5(a) shows the thermal profiles in the substrate. The temperature at the coating-substrate interface reached about 1273 K (1000 °C), which is lower than the temperature experienced by the coating [1573 K (1300 °C)]. When the hot plasticized metal touched the warm substrate, there was a drop in temperature. This thermal cycling altered the substrate top surface microstructure. Figure 5(b) shows the microstructure corresponding to different locations in the substrate, as indicated in the thermal profile. The microstructure in region "a" [1173 K to 1273 K (900 °C to 1000 °C)] reveals that the material was subjected to a considerable amount of plastic deformation, but it has not participated in the material transfer process. The microstructure at this region corresponds to upper bainite. At region "b" [1023 K to 1173 K (750 °C to 900 °C)], carbon-rich pearlite areas were austenized while the ferrite was not transformed. Region "c" experienced a temperature between 923 K and 1023 K (650 °C and 750 °C), where the cementite appears in spheroid morphology. Region "d" show the unaffected substrate base metal exhibiting a typical pancake structure.

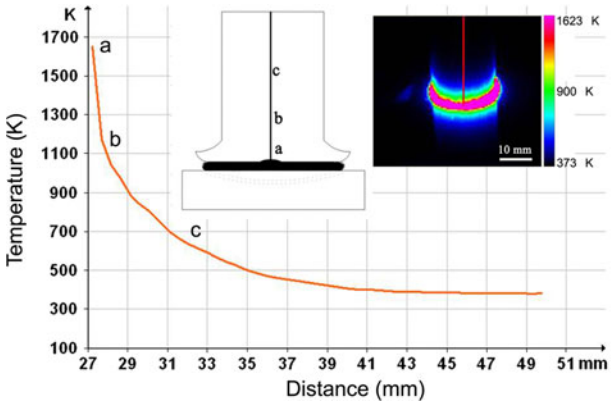

Fig. 4—Surface temperature distribution, along the line as indicated in the thermogram, in AISI 304 consumable rod.

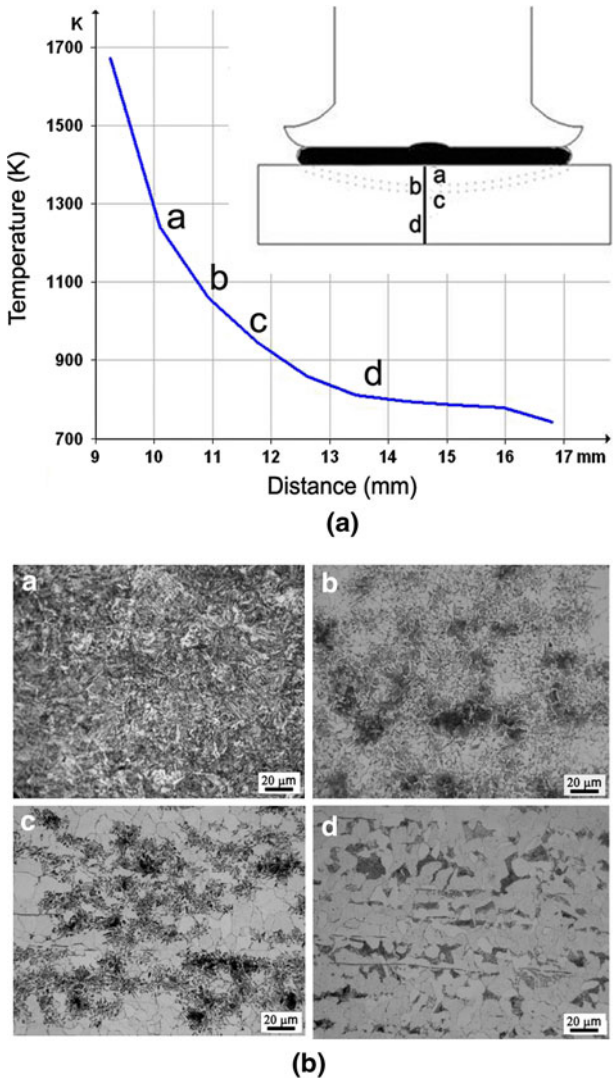

Fig. 5—(*a*) Plot of temperature distribution in the low carbon steel substrate. (*b*) Microstructure corresponding to locations indicated by letters "a" through "d" in the plot.

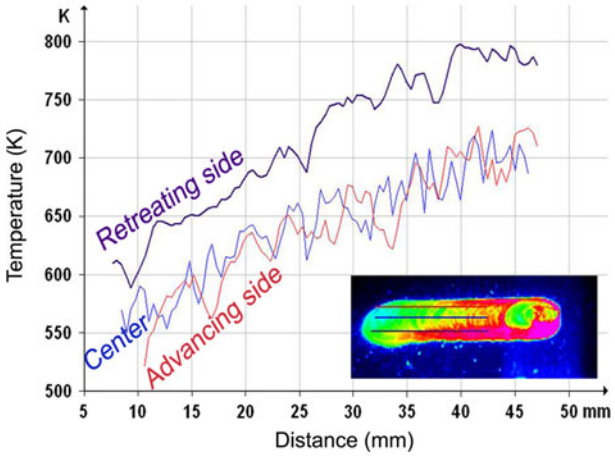

Fig. 6—Thermal profile on the retreating, center, and advancing side (the corresponding thermogram is shown in the inset).

Owing to the pattern of metal flow during the coating process,[16] a temperature difference can be expected on either side of the coating. Figure 6 shows the thermal profiles along a line on the advancing side, retreating side, and center. The thermal profiles reveal that the temperatures measured along the center and advancing sides are comparable, whereas the temperature at the retreating side is higher. This can be attributed to the flow of hot plasticized material from the advancing side to the retreating side, as suggested by an earlier study using the tracer particle technique.[16] However, this difference in temperature did not significantly influence the coating microstructure between the advancing and retreating sides.[17]

VI. CONCLUSIONS

IR thermography was used for the first time to generate thermal profiles during friction surfacing. The time-dependent heat generation during friction surfacing was clearly demonstrated. The sudden rise in temperature and attainment of steady state during the process is a result of viscous heat dissipation during plastic deformation, and the duration is short enough to be approximated as adiabatic. The thermal cycles involved in the process cause microstructural changes in substrate as well as in the consumable rod. The retreating side shows a higher temperature when compared to the advancing side and can be attributed to the flow of hot plasticized metal from the advancing side to the retreating side.

REFERENCES

1. A.W. Batchelor, S. Jana, C.P. Koh, and C.S. Tan: *J. Mater. Process. Technol.*, 1996, vol. 57, pp. 172–81.
2. G. Madhusudhan Reddy, K. Srinivasa Rao, and T. Mohandas: *Surf. Eng*, 2009, vol. 25 (1), pp. 25–30.
3. H. Thoman and B. Frisk: *Int. J. Heat Mass Transfer*, 1968, vol. 2, pp. 819–26.
4. C. Meola and G.M. Carlomagno: *Meas. Sci. Technol.*, 2004, vol. 15, pp. 27–58.
5. S. Matte, D. Grevey, A. Mathieu, and L. Kirchner: *Opt. Laser Technol.,* 2009, vol. 41, pp. 665–70.
6. R.S. Huang, L.M. Liu, and G. Song: *Mater. Sci. Eng. A*, 2007, vol. 447, pp. 239–43.
7. G. Bruggemann, A. Mahrle, and T. Benziger: *NDT&E Int*., 2000, vol. 33, pp. 453–63.
8. A. Mathieu, S. Mattei, A. Deschamps, B. Martin, and D. Grevey: *NDT&E Int*., 2006, vol. 39, pp. 272–76.
9. M.L. Pastor, X. Balandraud, M. Gre′diac, and J.L. Robert: *Infrared Phys. Technol*., 2008, vol. 51, pp. 505–15.
10. S. Paoloni, M.E. Tata, F. Scudieri, F. Mercuri, M. Marinelli, and U. Zammit: *Appl. Phys. A*, 2010, vol. 98, pp. 461–65.
11. S. Marinetti and V. Vavilov: *Corros. Sci*., 2010, vol. 52, pp. 865–72.
12. G.M. Bedford, V.I. Vitanov, and I.I. Voutchkov: *Surf. Coat. Technol*., 2001, vol. 14, pp. 134–39.
13. X.M. Liu, Z.D. Zou, Y.H. Zhang, S.Y. Qu, and X.H. Wang: *Surf. Coat. Technol*., 2008, vol. 202, pp. 1889–94.
14. R. Nandan, T. DebRoy, and H.K.D.H. Bhadeshia: *Prog. Mater. Sci*., 2008, vol. 53, pp. 980–1023.
15. G.A. Kluitenberg: *Physica*, 1967, vol. 35, pp. 177–92.
16. H. Khalid Rafi, G. Phanikumar, and K. Prasad Rao: *Metall. Mater. Trans. A*, 2011, vol. 42A, pp. 937–39.
17. H. Khalid Rafi, G.D. Janaki Ram, G. Phanikumar, and K. Prasad Rao: *Mater. Des*., 2011, vol. 32, pp. 82–87.